

Complex band structure with ultrasoft pseudopotentials: fcc Ni and Ni nanowire

A. Smogunov,^{1,2} A. Dal Corso,^{1,2} and E. Tosatti^{1,2,3}

¹SISSA, Via Beirut 2/4, 34014 Trieste (Italy)

²INFM, Democritos Unità di Trieste Via Beirut 2/4, 34014 Trieste (Italy)

³ICTP, Strada Costiera 11, 34014 Trieste (Italy)

(Dated: September 27, 2018)

We generalize to magnetic transition metals the approach proposed by Choi and Ihm for calculating the complex band structure of periodic systems, a key ingredient for future calculations of conductivity of an open quantum system within the Landauer-Buttiker theory. The method is implemented with ultrasoft pseudopotentials and plane wave basis set in a DFT-LSDA ab-initio scheme. As a first example, we present the complex band structure of bulk fcc Ni (which constitutes the tips of a Ni nanocontact) and monatomic Ni wire (the junction between two tips). Based on our results, we anticipate some features of the spin-dependent conductance in a Ni nanocontact.

INTRODUCTION

Recent conductance data of nanocontacts and break junctions in magnetic transition metals such as Ni have shown interesting and partly unexpected results. While early conductance histograms for Ni at room temperature in air appeared basically structureless [1], Oshima et al. [2], who worked in vacuum, at variable temperature, and with the possibility of a magnetic field, found a minimal conductance step preferentially near 2 and 4 (in units of $g_0 = e^2/h$, the conductance quantum per spin) at RT and zero field, near 4 at 770 K and zero field, and near 3 (occasionally near 1) at RT with a field. Ono et al. [3], reported again 2 for Ni in zero field, and 1 for Ni in a field. Break junction data by Yanson [4] show a minimal conductance step of about 3.2 in zero field. Despite the poor consistency between these data, it is clear that the lowest conductance step for a Ni nanocontact is anomalously small in comparison with the large expected number of $s+d$ conducting channels, of the order of at least 8 [5] for a monatomic contact.

In a previous paper [5] we investigated the possibility that the smallness of the last conductance step observed for a Ni nanocontact may be caused by the fact that two tips are magnetized in different directions forming a magnetization reversal (or domain wall) precisely in the contact region. By replacing the contact with a monatomic infinite tipless Ni wire we found that the number of conducting channels (energy bands crossing the Fermi level) can be significantly reduced from 8 (nonmagnetic wire) or 7 (ferromagnetic wire) to 2 as a magnetization reversal is built into the wire. The two remaining conducting channels correspond to light s -electrons, while the heavy d -electrons are confined in the regions of positive and negative magnetization and cannot propagate along the wire due to the magnetization reversal.

The real nanocontact consisting of two macroscopic tips and an atomic contact region is an open quantum system and has no artificial periodic conditions such as those in Ref.[5]. The influence of the tips themselves (not

considered in the previous model) will be in general important for the nanocontact conductance. So, in order to make quantitative conductance predictions one will need to adopt a more detailed approach comprising two semi-infinite metals (either thick wires or semi-infinite crystals) connected by a neck (a short monatomic wire, or just a single atom). Several theoretical methods are available to study the transport properties of atomic scale conductors. Among these are methods based on nonequilibrium Green's functions combined with a localized basis set [6, 7]. The Landauer-Buttiker formula provides another simple way to calculate the conductance of quantum systems connected to two tips. The conductance is expressed in terms of the transmission coefficient at the Fermi level E_F . In order to compute the transmission coefficient one must solve a scattering problem for the open quantum system. The scattering approach has been applied by Lang and co-workers [8], and Tsukada and co-workers [9, 10] using the jellium model for the electrodes. The layer KKR approach has been used to study the spin-dependent tunneling in magnetic tunnel junctions [11]. Lately Wortmann and co-workers [12] have formulated the transfer matrix approach based on computation of single-electron Green function in the linearized augmented plane wave (LAPW) basis. We are interested in a formulation based on plane waves and ultrasoft pseudopotentials, a calculational technology which we are applying to other problems involving transition metals [13] with great potential for the future.

Recently Choi and Ihm [14] presented a first-principles plane wave based solution to the scattering problem with real atomic contacts incorporating the Kleinman-Bylander-type pseudopotentials. We wish to generalize this scheme to deal with ultrasoft pseudopotentials [15] which adequately describe the nuclei and core electrons of a transition metal such as Ni. The first step, on which we focus in this paper is the complex band structure of periodic system, consisting of both propagating and exponentially decaying evanescent states. These generalized Bloch states will be needed to construct the scattering state deep inside the tips. The evanescent states play a

significant role in contact, surface or interface phenomena where there is a breaking of translational symmetry in one direction.

We present here the complex band structure of bulk Ni (which gives information on the nanocontact tips) and of a monatomic Ni wire (the junction between the two tips). Although this is clearly only the first step towards a full theoretical description of the nanocontact conductivity, we shall see that some insight can be obtained already by examining the complex bands. The importance of complex band structure for conductance predictions has been recently emphasized for magnetic tunnel junctions [16] and molecular systems [17].

METHOD

We consider an open quantum system divided into three regions: left bulk contact ($z < 0$), scattering region ($0 < z < L$) and right bulk contact ($z > L$) and we use a supercell geometry in the xy direction perpendicular to the wire. A wave propagating at energy E with $\mathbf{k} = (\mathbf{k}_\perp, k)$ and incident from the left contact on the scattering region will form a scattering state Ψ which due to the supercell geometry has a Bloch form in the xy direction:

$$\Psi_{\mathbf{k}_\perp}(\mathbf{r}_\perp + \mathbf{R}_\perp, z; \sigma) = e^{i\mathbf{k}_\perp \mathbf{R}_\perp} \Psi_{\mathbf{k}_\perp}(\mathbf{r}_\perp, z; \sigma). \quad (1)$$

Different \mathbf{k}_\perp do not mix and can be considered separately. If there is no coupling between different spin polarizations in the Hamiltonian the same conclusion is valid also for the spin index σ and we can omit both \mathbf{k}_\perp and σ from the following formulas.

Deep within the contacts the system becomes periodic also along the z direction and one can determine generalized Bloch states with complex k vector which obey to the periodic condition:

$$\psi_k(\mathbf{r}_\perp, z + d) = e^{ikd} \psi_k(\mathbf{r}_\perp, z), \quad (2)$$

where d is the length of the periodic unit cell deep within the contacts. In this region the scattering state Ψ can be written as a combination of propagating and evanescent generalized Bloch states:

$$\Psi = \begin{cases} \psi_k + \sum_{k' \in L} r_{kk'} \psi_{k'}, & \text{in the left tip} \\ \sum_{k' \in R} t_{kk'} \psi_{k'}, & \text{in the right tip} \end{cases}$$

where summation over $k' \in L$ ($k' \in R$) includes the generalized Bloch states in the left (right) contact at energy E which propagate or decay to the left (right). In the xy plane the wave functions $\psi_{k'}$ obey the same Bloch condition as in Eq.(1). Thus to compute the transmission and reflection coefficients $\{t_{kk'}, r_{kk'}\}$ one will need to find the complex band structure and generalized Bloch states ψ_k in the metallic contacts at the chosen energy E .

We determine here the complex band structure within Density Functional Theory (DFT) describing the atoms with ultrasoft pseudopotentials [15]. We consider the generalized Bloch states which satisfy the single-particle Kohn-Sham equation [18] (atomic units $e^2 = 2m = \hbar = 1$ are used):

$$E\hat{S}|\psi_k\rangle = \left[-\nabla^2 + V_{\text{eff}} + \hat{V}_{NL} \right] |\psi_k\rangle, \quad (3)$$

where V_{eff} is the effective local potential (see Ref. [15, 18]), V_{NL} is the nonlocal part of the ultrasoft pseudopotential:

$$\hat{V}_{NL} = \sum_{Imn} D_{mn}^I |\beta_m^I\rangle \langle \beta_n^I|, \quad (4)$$

constructed using the set of projector functions β_m^I associated with atom I and \hat{S} is the overlap operator:

$$\hat{S} = 1 + \sum_{Imn} q_{mn}^I |\beta_m^I\rangle \langle \beta_n^I|. \quad (5)$$

The coefficients q_{mn}^I are the integrals of the augmentation functions defined in Ref. [15, 18]. It is convenient to rewrite Eq. (3) in the form:

$$\begin{aligned} E|\psi_k\rangle &= \left[-\nabla^2 + V_{\text{eff}} \right] |\psi_k\rangle \\ &+ \sum_{Imn} (D_{mn}^I - E q_{mn}^I) |\beta_m^I\rangle \langle \beta_n^I| \psi_k. \end{aligned} \quad (6)$$

From this equation it can be seen that the scattering problem in the ultrasoft pseudopotential case is not substantially different from the norm conserving one (where E does not appear on the r.h.s.) since the energy E is fixed and is given as an external parameter.

As in Ref. [14] we can write the solution of the integro-differential Eq. (6) as a linear combination:

$$\psi_k(\mathbf{r}) = \sum_n a_{n,k} \psi_n(\mathbf{r}) + \sum_{Im} c_{Im,k} \psi_{Im}(\mathbf{r}), \quad (7)$$

where ψ_n are linearly independent solutions of the homogeneous equation:

$$E\psi_n(\mathbf{r}) = \left[-\nabla^2 + V_{\text{eff}}(\mathbf{r}) \right] \psi_n(\mathbf{r}), \quad (8)$$

and ψ_{Im} is a particular solution of the inhomogeneous equation:

$$\begin{aligned} E\psi_{Im}(\mathbf{r}) &= \left[-\nabla^2 + V_{\text{eff}}(\mathbf{r}) \right] \psi_{Im}(\mathbf{r}) \\ &+ \sum_{\mathbf{R}_\perp} e^{i\mathbf{k}_\perp \mathbf{R}_\perp} \beta_m^I(\mathbf{r} - \mathbf{r}^I - \mathbf{R}_\perp). \end{aligned} \quad (9)$$

Both ψ_n and ψ_{Im} are (x, y) periodic as in Eq. (1). Summation over Im in Eq. (7) involves all the projectors in the unit cell and the coefficients $c_{Im,k}$ are determined by:

$$c_{Im,k} = \sum_n [D_{mn}^I - E q_{mn}^I] \int [\beta_n^I(\mathbf{r} - \mathbf{r}^I)]^* \psi_k(\mathbf{r}) d^3r. \quad (10)$$

Note that the set of wave functions ψ_n is infinite. In practice the expansion $\psi_n(\mathbf{r}) = \sum_{\mathbf{G}_\perp} \psi_n(\mathbf{G}_\perp, z) e^{i(\mathbf{k}_\perp + \mathbf{G}_\perp) \cdot \mathbf{r}_\perp}$ over two-dimensional plane waves is used. If one considers only N_{2D} plane waves with $\mathbf{G}_\perp^2 \leq E_{\text{cut}}$ the number of ψ_n becomes finite and equals to $2N_{2D}$. As in Ref.[14] to find the functions ψ_n we discretize the unit cell along the z axis by dividing it into slices and replacing the $V_{\text{eff}}(\mathbf{r})$ in each slice by a z -independent potential. The ψ_n in the slices will be a linear combination of two exponentials with coefficients obtained by a matching procedure.

The allowed values of k for a given energy E can be determined by imposing periodicity along z (Eq. (2)) to the generalized Bloch function $\psi_k(\mathbf{r}) = \sum_{\mathbf{G}_\perp} \psi_k(\mathbf{G}_\perp, z) e^{i(\mathbf{k}_\perp + \mathbf{G}_\perp) \cdot \mathbf{r}_\perp}$ and to its z derivative:

$$\psi_k(\mathbf{G}_\perp, d) = e^{ikd} \psi_k(\mathbf{G}_\perp, 0). \quad (11)$$

$$\psi'_k(\mathbf{G}_\perp, d) = e^{ikd} \psi'_k(\mathbf{G}_\perp, 0). \quad (12)$$

Inserting Eq. (7) into Eqs. (10)-(12) one can show that the last three equations are equivalent to the generalized eigenvalue problem:

$$AX = e^{ikd} BX. \quad (13)$$

where A and B are matrices. We solve this problem to obtain in general a complex k and coefficients $X = \{a_{n,k}, c_{Im,k}\}$ for the generalized Bloch state ψ_k at a given energy E and \mathbf{k}_\perp .

Our complex band structure calculations proceed in two steps. First we compute with a standard electronic structure code (PWSCF) [21] the ground state electronic structure of the system (infinite bulk; and, separately, infinite perfect nanowire) and we obtain the effective local potential $V_{\text{eff}}(\mathbf{r})$ and the screened coefficients D_{mn}^I [22]. In a second step, we use the potential $V_{\text{eff}}(\mathbf{r})$ and the screened coefficients D_{mn}^I to compute the complex band structure applying the scheme described above [23].

RESULTS AND DISCUSSION

As a first example, we studied the complex band structure of ferromagnetic bulk fcc Ni (Fig.1). The orientation of the Ni tips in the actual break junction experiments is not under control, and we have chosen to plot the complex bands appropriate for a (001) orientation of the electrodes. We considered a tetragonal unit cell with two nickel atoms and the z axis parallel to the tetragonal axis. Our calculated optimal equilibrium lattice constant of ferromagnetic fcc Ni is $a = 3.42 \text{ \AA}$ (expt. $a = 3.52 \text{ \AA}$) and this value has been used for the band structure calculation. At this volume the magnetic moment per atom is $0.59 \mu_B$ (expt. $0.61 \mu_B$) [24]. In the scattering problem we took $\mathbf{k}_\perp = 0$ for the purpose of exemplification. Due to the symmetry of the Hamiltonian [25], if at a fixed

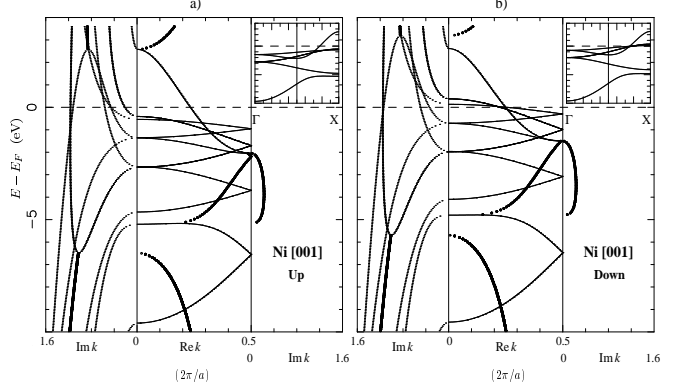


FIG. 1: Complex band structure of fcc Ni along [001] direction at $\mathbf{k}_\perp = 0$ for the majority (spin up) and minority (spin down) states. Tetragonal unit cell containing two atoms was used. Real bands (solid curves), complex bands with $\text{Re } k = 0$ (dotted curves) are plotted in the middle and left panels, respectively. The real projection of complex bands (open circles) is plotted in the middle panel, and the corresponding imaginary projection (open circles) is plotted in the left or right panels. The band structures along Γ -X direction in the fcc Ni are shown on the insets.

energy E a real k is a solution of the problem, also $-k$ is a solution (corresponding to right- and left- propagating waves). If a complex k is a solution also $-k, k^*, -k^*$ are solutions [25] (states with $\text{Im } k > 0$ ($\text{Im } k < 0$) correspond to evanescent modes decaying along the positive (negative) z direction). We can therefore show the complex band structure just in the region $\text{Re } k \geq 0$ and $\text{Im } k \geq 0$.

Ni is a ferromagnetic metal and we plot in Fig. 1a and 1b the bands corresponding to the majority spin (spin up) and minority spin (spin down) respectively. Figs. 1a and 1b are divided into three panels. The propagating bands with $\text{Re } k \neq 0$ and $\text{Im } k = 0$ are plotted with continuous lines in the central panel. Dotted lines in the left panel represent bands with purely imaginary k ($\text{Re } k = 0$ and $\text{Im } k \neq 0$). The bands which correspond to complex k with $\text{Re } k \neq 0$ and $\text{Im } k \neq 0$ are represented with open circles. They are shown with two branches which correspond to their projection in the real and imaginary planes. We chose arbitrarily to plot the projection on the imaginary plane in the left or in the right part of the figure in order to improve clarity. The band structure of fcc Nickel corresponding to real k obtained with PWSCF are shown in the inset of Fig. 1 along the Γ - X direction. Since our cell has two atoms, the bands with real k in Fig.1 should coincide with the one in the inset after folding about the middle vertical line. We indeed found excellent agreement between the real band structures in the two calculations, with differences of the order of 0.005 eV (invisible in the figure).

In the band structure of fcc Ni one can identify five narrow 3d bands and one broader 4s band. Along the

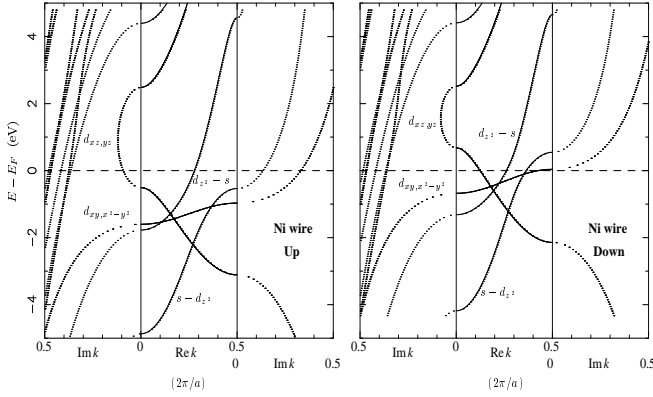


FIG. 2: Complex band structure of monatomic Ni wire for the majority (spin up) and minority (spin down) states. Real bands (solid curves), complex bands with $\text{Re } k = 0$, and π/a (dotted curves) are plotted in the middle, left, and right panels, respectively. Each band is labeled by its main atomic character.

(001) direction the s band mixes with the d_{z^2} band. The spin up d bands are fully occupied and only the $s - d_{z^2}$ band crosses the Fermi level. The down spin d bands are upshifted in energy by a calculated exchange splitting of about 0.5 eV (exp. 0.33 eV). Therefore they are partially unoccupied and three d states in addition to the $s - d_{z^2}$ state crosses the Fermi level. The complex bands shown in Fig.1 can be interpreted in terms of general theorems which describe their topological features [25]. It is known that whenever a band with real k has a local extremum there is a complex band with opposite curvature and the same symmetry which departs at the same $\text{Re } k$ at right angles from the real plane. Complex k bands are parabolic or form loops joining real bands of the same symmetry. One such loop in the complex plane joins $s - d_{z^2}$ bands connecting the maximum at $\text{Re } k = 0.18$ ($2\pi/a$) (very weakly pronounced) with the minimum at $k = 0.5$ ($2\pi/a$). Comparing the complex band structures for different spin polarizations one can notice that there are four propagating spin down bands at E_F while for spin up polarization the d bands cross the Fermi level only in the imaginary plane and are therefore evanescent (the smallest decay is $\text{Im } k = 0.2$ ($2\pi/a$)).

In Fig. 2 we show the complex band structure for a monatomic Ni wire ($a = 2.12$ Å). The supercell geometry and the other technical parameters used in this calculation were already discussed in Ref. [5]. The bands at real k coincide (within 0.005 eV) with those presented there and calculated with the PWSCF code. Here all the occupied real bands have maxima or minima at the zone border and the complex bands are therefore either purely imaginary (they are shown by dots in the left panel) or have $\text{Re } k = \pi/a$ (they are shown by dots in the right panel). Bands at imaginary k have a parabolic dispersion except for the loop which joins $d_{xz,yz}$ bands. As

in the case of bulk Ni at the Fermi energy there is only one real $s - d_{z^2}$ band of spin up polarization. All the d states are decaying and the smallest decay ($d_{xz,yz}$ states) is $\text{Im } k = 0.08$ ($2\pi/a$). On the contrary 6 spin down bands with real k cross the Fermi level and the only decaying states crossing the Fermi energy have a much larger imaginary part $\text{Im } k = 0.35$ ($2\pi/a$).

The asymmetry between energy bands at E_F for different spin directions and the existence of evanescent states with long decay lengths (small decay parameters $\text{Im } k$) will play an important role in transport properties of the magnetic nanocontacts. One can see, for example, that if there is no spin reversal (two tips and the wire are magnetized in the same direction) all propagating states coming from the bulk Ni can get (though with some reflection at the junctions) through the wire. On the other hand, if there is one spin reversal (situated either on one end of the wire or in the middle) the propagating d -electrons of one Ni tip become decaying in another Ni tip so that they will be completely blocked. The only open channels correspond to s -electrons (this conclusion was arrived at [5] considering a simple model of the Ni nanocontact). And, finally, in the hypothetical case of two spin reversals (when the wire has the opposite direction of magnetization with respect to both tips) the d -electrons are only able to tunnel across the wire through the evanescent states. The latter have an exponential decaying form $\psi_k \sim e^{-z/\ell}$ with the decay length $\ell = 7.96$ a.u. ($d_{xz,yz}$), 5.31 a.u. ($s - d_{z^2}$), and 2.0 a.u. (d_{xy,x^2-y^2}) which should be compared with the distance between atoms in the Ni wire $a = 4.0$ a.u. The shorter the wire, the larger the contribution of d -electrons to the total conductivity. This result is similar to the spin-dependent tunneling in magnetic tunnel junctions (see [11, 16]) although in our case it is not so crucial since two propagating s -channels always exist. All these ingredients will become crucial when one will solve the scattering problem in order to find the transmission coefficient. It should be emphasized that the number of propagating channels N give the upper limit for conductivity, $G = \frac{e^2}{h} N$ with unit transmission for all channels, while the scattering problem solution may produce very small transmission coefficients for some propagating channels. The channel number N of a thick wire will diverge proportional to the wire cross section, realizing the perfect conductance expected for a macroscopic case.

CONCLUSIONS

We are working to generalize to magnetic transition metals the approach proposed by Choi and Ihm for calculating the ballistic conductance of open quantum systems within the Landauer-Buttiker theory. In this paper we focused on the complex band structure of periodic systems, which is the key ingredient for the wave-function

matching between the scattering region and the metallic electrodes. The method has been implemented for the first time with ultrasoft pseudopotentials and plane waves in a DFT-LSDA ab-initio scheme. We showed that it can be applied to both the bulk solid and to the idealized monatomic nanowire. As a first application we calculated the complex band structure of fcc Ni and of a ferromagnetic Ni monoatomic wire and discussed qualitatively the properties of a nickel nanocontact which can be inferred from the complex band structure. Detailed calculations of conductance will be undertaken in forthcoming work.

ACKNOWLEDGMENTS

This work was partly sponsored by MIUR PRIN, by INFM (section F, G, PRA NANORUB and “Iniziativa Trasversale calcolo parallelo”), and EU Contract ERBFMRXCT970155 (FULPROP). Some calculations were performed on the IBM-SP3 at CINECA, Casalecchio (Bologna).

[1] J.L. Costa-Kramer, Phys. Rev. B **55**, R4875 (1997).
 [2] H. Oshima and K. Miyano, Appl. Phys. Lett. **73**, 2203 (1998).
 [3] T. Ono, Yu. Ooka, and H. Miyajima, Appl. Phys. Lett. **75**, 1622 (1999).
 [4] A.I. Yanson *Atomic chains and electronic shells: quantum mechanisms for the formation of nanowires*, Ph.D. thesis, University of Leiden (2001).
 [5] A. Smogunov, A. Dal Corso, and E. Tosatti, Surf. Sci. **507**, 609 (2002).
 [6] M. Brandbyge, J.-L. Moroz, P. Ordejon, J. Taylor, and K. Stokbro, Phys. Rev. B **65**, 165401 (2002).
 [7] B. Larade, J. Taylor, and H. Guo, Phys. Rev. B **64**, 075420 (2001).
 [8] N.D. Lang, Phys. Rev. B **52**, 5335 (1995).
 [9] K. Hirose and M. Tsukada, Phys. Rev. B **51**, 5278 (1995).
 [10] N. Kobayashi, M. Brandbyge, and M. Tsukada, Phys. Rev. B **62**, 8430 (2000).
 [11] J.M. MacLaren, X.-G. Zhang, W.H. Butler, and X. Wang, Phys. Rev. B **59**, 5470 (1999); M. Freyss, N. Papanikolaou, V. Bellini, R. Zeller, and P.H. Dederichs, Phys. Rev. B **66**, 014445 (2002); W.H. Butler, X.-G. Zhang, T.C. Schulthess, and J.M. MacLaren, Phys. Rev. B **63**, 054416 (2001).
 [12] D. Wortmann, H. Ishida, and S. Blugel, Phys. Rev. B **65**, 165103 (2002).
 [13] A. Dal Corso, Phys. Rev. B **64**, 235118 (2001) and references therein; E. Tosatti, S. Prestipino, S. Kostlmeier, A. Dal Corso, and F. Di Tolla, Science **291**, 288 (2001).
 [14] H.J. Choi and J. Ihm, Phys. Rev. B **59**, 2267 (1999).
 [15] D. Vanderbilt, Phys. Rev. B **41**, 7892 (1990).
 [16] Ph. Mavropoulos, N. Papanikolaou, and P.H. Dederichs, Phys. Rev. Lett. **85**, 1088 (2000).
 [17] John K. Tomfohr and Otto F. Sankey, Phys. Rev. B **65**, 245105 (2002).
 [18] K. Laasonen, A. Pasquarello, R. Car, Ch. Lee, and D. Vanderbilt, Phys. Rev. B **47**, 10142 (1993).
 [19] J. Perdew and A. Zunger, Phys. Rev. B **23**, 5048 (1981).
 [20] M. Methfessel and A.T. Paxton, Phys. Rev. B **40**, 3616 (1989).
 [21] S. Baroni, A. Dal Corso, S. de Gironcoli, and P. Giannozzi, <http://www.pwscf.org>.
 [22] The calculations are based on local spin density approximation (LSDA) with the Perdew-Zunger parametrization [19] of exchange-correlation energy. The nuclei and the core electrons are described by ultrasoft pseudopotentials with the parameters of Ref. [5]. The kinetic energy cut-offs of the plane wave basis set were 25 Ry and 300 Ry for the wave functions and the charge density, respectively. \mathbf{k} -point sampling is done with 60 points in the irreducible BZ for bulk Ni and with a uniform mesh of 40 \mathbf{k} -points in the 1D BZ zone for the Ni wire. The integration up to the Fermi level was done by a standard broadening technique [20] with the smearing parameter of 0.005 Ry.
 [23] The 2D cut-off energy was taken as in electronic structure calculations and the number of slices was 24 for bulk Ni and 15 for Ni wire (in both cases the slice thickness is about 0.14 Å) which proved sufficient to represent the shape of the potential $V_{\text{eff}}(\mathbf{r})$.
 [24] A. Dal Corso and S. de Gironcoli, Phys. Rev. B **62**, 273 (2000).
 [25] Y.-C. Chang, Phys. Rev. B **25**, 605 (1982).